LIMNOLOGY and OCEANOGRAPHY

ASLO

Limnol. Oceanogr. 66, 2021, 3221–3236

doi: 10.1002/lno.11875

Analysis of coastal storm damage resistance in successional mangrove species

Rosanna van Hespen,[1,2] **Zhan Hu**,[3,4,5*] **Yisheng Peng**,[6] **Bas W. Borsje**,[7] **Maarten Kleinhans**,[2] **Tom Ysebaert**,[1,8] **Tjeerd J. Bouma**[1,2]

[1]Department of Estuarine and Delta Systems, NIOZ Yerseke, Royal Netherlands Institute for Sea Research and Utrecht University, Yerseke, The Netherlands
[2]Department of Physical Geography, Faculty of Geosciences, Utrecht University, Utrecht, The Netherlands
[3]School of Marine Science, Sun Yat-Sen University, and Southern Marine Science and Engineering Guangdong Laboratory (Zhuhai), Zhuhai, China
[4]Guangdong Provincial Key Laboratory of Marine Resources and Coastal Engineering, Guangzhou, China
[5]Pearl River Estuary Marine Ecosystem Research Station, Ministry of Education, Zhuhai, China
[6]School of Environmental Science and Engineering, Sun Yat-Sen University, Guangzhou, China
[7]Water Engineering and Management, University of Twente, Enschede, The Netherlands
[8]Wageningen University & Research, Wageningen Marine Research, Yerseke, The Netherlands

Abstract

Use of mangrove ecosystems for coastal flood protection requires reliable predictions of mangrove wave attenuation, especially if this capacity lessens due to storm-induced forest damage. Quantifying and understanding the variation in drag forces and mechanical properties of mangrove vegetation can improve assessment of mangrove protective capacity. We studied five mangrove species common in the subtropical Pearl River Delta, south China. The studied species range from typically landward-occurring to more seaward-occurring pioneer species. We sampled across seven sites in the delta to study the impact of salinity on mechanical properties. We quantified strength and flexibility of branches (branch strength and flexibility related to branch diameter, modulus of rupture and modulus of elasticity), leaf strength (leaf attachment strength related to leaf size, and leaf mass per area) and drag properties (drag force related to surface area and drag coefficient). For all tested species, larger branch diameters resulted in higher mechanical strength. Larger leaf size resulted in larger peak pulling forces and larger branch surface area resulted in stronger drag forces. Notably, species that generally occur lower in the intertidal zone, where exposure to wind and waves is higher, had relatively stronger branches but more easily detachable leaves. This may be regarded as a damage-avoiding strategy. Across the seven field sites, we found no clear effect of salinity on mangrove mechanical properties. This study provides a mechanistic insight in the storm damage process for individual mangrove trees and a solid base for modeling storm (surge) damage at the forest scale.

Reducing cost of flood protection with coastal ecosystems

The urgency for effective and affordable coastal flood defense will increase if sea levels and storm frequency rise as projected over the coming decades (Knutson et al. 2019; Nicholls et al. 2019). This is especially the case in highly urbanized deltas, such as the Pearl River Delta in south China, that harbors megacities like Guangzhou and Shenzhen (De Dominicis et al. 2020). The cost of maintaining coastal safety increases as larger barrier structures are needed. Coastal vegetation can attenuate waves, reducing the required height of barrier structures and resulting in lower construction and maintenance costs (Borsje et al. 2011; Temmerman et al. 2013). Consequently, coastal ecosystems are increasingly considered as an addition to conventional coastal safety structures (Temmerman et al. 2013; van Wesenbeeck et al. 2017; Morris et al. 2019). In subtropical and tropical areas, mangrove forests are known for the large extent of ecosystem services they can provide, and their dense vegetation and high elevation in the intertidal zone makes them effective natural wave attenuating structures (Bouma et al. 2014; Lee

*Correspondence: huzh9@mail.sysu.edu.cn

Additional Supporting Information may be found in the online version of this article.

et al. 2014). Under the right circumstances, they may even attenuate extreme storm waves, provided that vegetation stretches wide and matches the height and length of the waves (Bao 2011; Horstman et al. 2014; Menéndez et al. 2020). However, mangroves are dynamic, living structures that do not always have the same vegetation width and density. Supplementing conventional coastal safety structures with mangrove ecosystems will require a strong understanding of how mangrove width and density fluctuate, to enable careful prediction and testing of the long-term structural integrity of these ecosystems (Bouma et al. 2014).

Variability in flood protection by mangrove forests

The coastal wave attenuating capacity of mangrove ecosystems is related to surge properties and to the size, height and density of the vegetated area: a larger, denser forest leads to better protection, and vegetation height relative to the storm surge determines what part of the vegetation (pneumatophores, tree trunks, canopy) can attenuate waves (Mazda et al. 1997; Bouma et al. 2014; McIvor et al. 2015). For example, height of native species in the Pearl River Delta in south China is comparable to the seawalls behind them and can thus experience waves over the full height of the tree during storms (Fig. S1). Naturally, these vegetation properties are variable across species, age and space inside and across forests (i.e., canopy height is globally related to precipitation, temperature and cyclone frequency; Koch et al. 2009; Simard et al. 2019). Furthermore, large irregular disturbances can strongly impact forest structure and consequently wave attenuation capacity as well as long-term presence. If disturbance regimes such as storm frequency or intensity are altered under climate change (Hoegh-Guldberg et al. 2018; Knutson et al. 2019), this could drive forests that are already vulnerable from previous disturbances over an ecological tipping point, resulting in substantial narrowing or loss of the ecosystem (Scheffer et al. 2001; Bouma et al. 2014). Even if forest size is relatively stable, recovering will take some time, during which local protection capacity is lowered (Johnstone et al. 2016; Krauss and Osland 2020). Conventional flood protection structures need to adhere to rigid safety standards, often measured to withstand a storm of particular intensity, that has an estimated return period (e.g., 100 years; CIRIA et al. 2013). To safely integrate mangroves in flood protection schemes, it is essential to understand how mangrove vegetation structure changes under disturbance regimes.

Mechanistic models for storm damage predictions

Storms and accompanying storm surges can cause mangrove tree damage through direct mechanical impact such as branch and trunk damage and complete defoliation, and indirect effects like extensive flooding and displacement of large volumes of sediment (Jimenez et al. 1985; Smith et al. 1994; Ouyang et al. 2021). Predicting direct mechanical storm damage in forests can be done with models like HWIND, FOREOLE, and GALES (Gardiner et al. 2008). Such models can predict tree uprooting and trunk breakage by comparing tree strength with drag force generated in local (storm) wind climates (Peltola et al. 1999). Mangroves can experience damage from both wind and waves during coastal storms. For example, Tanaka (2008) observed tree damage similar to that of damage by tsunamis or river floods after Cyclone Sidr hit Bangladesh in 2007. These existing storm damage models have been developed for trees in terrestrial forests and do not incorporate the impact of water motion that may impose much larger drag forces (a drag force imposed by water moving at a velocity of 2 $m\ s^{-1}$ is roughly equivalent to wind speeds of 130 mph or 58.3 $m\ s^{-1}$; Denny and Gaylord 2002). Still, the basic principle remains: a force is acting on a tree. Thus, the modeling principle may also be applied in the case of storm surge damage on mangroves, where wind is replaced with waves and terrestrial wood properties are replaced by mangrove wood properties.

Variability in storm damage across species and space

When making mechanistic predictions of mangrove tree damage, it should be considered that not all trees are damaged in the same way. For instance, it is known that tree species vary in their mechanical strength (Chave et al. 2009; Santini et al. 2013) and mechanical flexibility (where more flexible wood can reduce storm impact; Kauffman and Cole 2010). Furthermore, leaf mechanical properties such as leaf size, which increases drag force acting on the tree, and the potential for leaf reorientation and defoliation under influence of wind and waves (which reduce surface area and resulting drag force), vary across plant species (Vollsinger et al. 2005; Onoda et al. 2011; Butler et al. 2012). These differences often follow drag avoidance or drag tolerance strategies, such that some species, often pioneers, are better equipped to deal with the force of incoming surge waves (e.g., in saltmarshes, seaward pioneers have more flexible stems, which helps to reduce drag; Schoutens et al. 2020; Puijalon et al. 2011). Beyond species differences, environmental factors may also affect the mechanical properties of mangrove trees. Wood density—which correlates positively with mechanical strength (Chave et al. 2009)—differs across intertidal position, countries (Santini et al. 2012), and possibly salinity (Table S1). Given these potential sources of variation, predicting storm impact on mangroves requires sufficient knowledge of mechanical and drag properties across mangrove species and environmental variables.

Aims of this research

Safely integrating mangrove forests in coastal protection schemes requires accurate predictions of forest size and structure under the influence of storms. Here, we focus on identifying storm surge resistance of mangrove trees by quantifying the mechanical and drag properties of small branches (0.5–

1.75 cm diameter) and leaves of five species. We situate the study in the Pearl River Delta, one of the largest urban deltas in the world that could benefit from nature-based flood protection with mangroves (De Dominicis et al. 2020; Menéndez et al. 2020). The five species studied here are common in the Pearl River Delta and range from typically seaward occurring with pioneer traits to more landward growing species with late-successional traits. We quantify the species' mechanical and drag properties across a salinity gradient along seven sites in the larger delta area. We quantify the following properties:

- strength and flexibility of mangrove branches (branch strength and flexibility related to branch diameter, modulus of rupture [MOR] and modulus of elasticity [MOE]),
- mangrove leaf strength (leaf attachment strength related to leaf size and petiole diameter, and leaf mass per area [LMA]), and
- drag properties (drag force related to surface area and drag coefficient).

The collected data are analyzed to assess: (1) potential damage avoidance strategies for different species and (2) possible salinity impact on mechanical properties. We do this to provide mechanistic insight in storm damages for individual mangrove trees across species and salinities, ultimately supporting the aim to improve predictions of mangrove-based flood safety.

Materials

We collected data on mechanical and drag properties of five mangrove species to estimate potential storm damage on individual trees (Table 1). These data comprise:

1. Strength and flexibility of small mangrove branches (diameters ranging from 0.5 to 1.75 cm, allowing us to harvest and transport branches from field to the lab without causing unacceptably large damage to trees). We measured strength as the absolute peak force (F_{max}, N) branches can withstand and flexibility as the amount of force needed to bend a branch a certain amount (e.g., 1 mm; F/x, $N\,mm^{-1}$). From this, we derived relative material properties independent of branch diameter: MOR ($N\,mm^{-2}$), a relative measure of strength, and MOE ($N\,mm^{-2}$), a relative measure of flexibility.
2. Leaf attachment strength (F_{pull}, N), where we measured the peak force required to detach a leaf under a static load and compared this to leaf size (leaf surface area A_{leaf}, cm^2), petiole diameter (cm), and cost of leaf production (LMA, $g\,cm^{-2}$).
3. Drag force on mangrove branches (F_D, N), where we measured drag force linked to branch surface area (A_{proj}, m^2) and derived a drag coefficient (C_D, dimensionless).

The mangrove species studied are typical for the subtropical Pearl River Delta. To identify potential differences in storm damage avoidance or resistance traits, we selected species that range from generally more sheltered, landward occurring to generally more exposed, seaward occurring pioneer species: *Acanthus ilicifolius*, *Kandelia obovata*, *Aegiceras corniculatum*, *Avicennia marina*, and *Sonneratia apetala*, listed here from landward to seaward, respectively. We selected seven field sites to cover salinities that range from freshwater to seawater (0–15 psu) to study the potential effect of salinity on mangrove mechanical properties.

Species and site selection

We collected data at seven locations in the Pearl River Delta, Guangdong province, south China. Between 1954 and 2008, 181 typhoons have landed in this province (Jie et al. 2012). During a typhoon, wave height can reach up to 2 m surge height can reach up to 4 m at the coast inside the Pearl River Delta (Yin et al. 2017; De Dominicis et al. 2020). The seven sites have increasing salinity ranging from 0 to 15 psu (Fig. 1; for salinity estimation *see* Supporting Information, Appendix S1). We sampled five species commonly found in the subtropical Guangdong province, south China: *A. ilicifolius*, *K. obovata*, *A. corniculatum*, *A. marina*, and *S. apetala* listed here as ranging from respectively high intertidal (landward species) to low intertidal (seaward species; based on Peng et al. [2016] and our own field observations). Particularly, *A. marina* and *S. apetala* are considered pioneer species in the region, *K. obovata* and *A. corniculatum* less so and *A. ilicifolius* is not considered a pioneer species (Ren et al. 2008; Chen et al. 2015). Note that *A. ilicifolius* is not a woody species, unlike the other four. In the Pearl River Delta, south China, these species do not reach tall heights (~2–4 m max.), except for the non-native species *S. apetala*, that reaches heights of ~5–12 m. The native species have heights comparable to the seawalls behind the mangrove forests (i.e., built to resist expected storm water levels), such that they can experience waves over the length of the full tree (Fig. S1). The non-native species *S. apetala* can be significantly higher than adjacent seawalls and may therefore be less effective in wave attenuation and more sensitive to wind forces. *S. apetala* is an exotic species in China and was introduced from Bangladesh for mangrove afforestation in the mid-1980s (Xin et al. 2013). Although some of the selected species have low salinity tolerance (*A. ilicifolius*: low, *K. obovata*: mid, *A. corniculatum*: mid, *A. marina*: high and *S. apetala*: low; Ye et al. 2005; Reef and Lovelock 2015), the 0–15 psu range is relatively low for mangroves in general and likely tolerable for all species—indeed, they grow at most sites (Fig. 1; but note that *S. apetala* trees are often nursery-raised and then planted; Ren et al. 2009).

Mechanical properties of mangrove branches

We collected branches at each site for one to five species, depending on availability (Fig. 1). Sampling was carried out from 9 to 24 January 2019. One or two branches were taken

Table 1. Mechanical and drag properties used with symbols and their meaning.

Item	Symbol	Unit	Name and explanation	Obtained by
Branch	F_{max}	N	Absolute peak force: Maximum load before branch breaks	Measured
Branch	F/x	N mm^{-1}	Flexibility: Initial slope of the stress–strain curve, i.e., force needed to bend the branch a certain amount (e.g., 1 mm)	Measured
Branch	R, $\emptyset$	cm	Branch radius, branch diameter	Measured
Branch	L	m	Branch arm: Length of the part of the branch that experiences load F	Measured
Branch	MOR	N mm^{-2}	MOR: a relative, size-independent measure of branch strength	$\mathrm{MOR} = \frac{F_{max} L}{\pi R^3}$
Branch	MOE	N mm^{-2}	MOE: a relative, size-independent measure of branch rigidity	$\mathrm{MOE} = \frac{F}{x} \times \frac{L^3}{12\pi R^4}$
Leaf	F_{pull}	N	Leaf attachment strength: Peak pulling force at which leaf detaches	Measured
Leaf	A_{leaf}	cm^2	Leaf size: Leaf surface area	Measured
Leaf	M_{leaf}	g	Leaf dry weight	Measured
Leaf	LMA	g cm^{-2}	Cost of leaf production: LMA, in gram biomass invested to produce 1 m^2 leaf, considered a measure of cost of leaf production	$\mathrm{LMA} = \frac{M_{leaf}}{A_{leaf}}$
Leaf	$\mathrm{MOL_A}$	N cm^{-2}	Modulus of leaf loss, area based: Force required to detach a leaf for a given leaf size	$\mathrm{MOL}_A = \frac{F_{pull}}{A_{leaf}}$
Leaf	$\mathrm{MOL_M}$	N g^{-1} cm^2	Modulus of leaf loss, mass based: Force required to detach a leaf for a given leaf cost (using LMA as measure of cost)	$\mathrm{MOL}_M = \frac{F_{pull}}{\mathrm{LMA}}$
Drag	F_D	N	Drag force experienced by branch	Measured
Drag	A_{proj}	m^2	Branch surface area: Projected frontal surface area of branch	Measured
Drag	u	m s^{-1}	Wave orbital velocity	Measured
Drag	ρ	Kg m^{-3}	Fluid density (1000 kg m^{-3} for freshwater)	Known constant
Drag	C_D	—	Drag coefficient	$C_D = \frac{2F_D}{\rho u^2 A_{proj}}$

from a tree, with diameters ranging between roughly 0.50 cm and about 1.75 cm (*see* Fig. S2 for branch diameters per hierarchy level). We selected this size range and excluded larger sizes for three reasons: (i) in several cases, taking larger branches would have resulted in destruction of a major part of or even the whole tree, (ii) large parts of tree biomass can be found in smaller branches (Fig. S2), as trees likely have more smaller than larger branches, and (iii) the MOR and MOE are size-independent measures for which diameter is not relevant (Fig. S3). Each tree was selected randomly but opportunistically, considering limited accessibility due to deep creeks or dense vegetation. For each required diameter, the straightest part of a branch was selected and stripped of any side branches such that it approximated a straight cylinder. This need not be the point where a branch will actually break during a storm, but it offered the best place to get reproducible measurements on location independent tissue properties such as MOR and MOE (Gere and Goodno 2009). These properties can then be used to calculate the actual strength at any place of a branch, assuming there are no weaknesses in the branch. Collected branches were then rolled in moist paper towels and stored in airtight bags in cool boxes with ice and transferred to a fridge upon arrival at the lab before analysis. Analysis using a three-point bending test happened within 48 h after collection of the branches.

The three-point bending test was carried out to obtain both absolute tissue properties—maximum load F_{max} (N) and force to bend F/x (N mm^{-1})—and relative tissue properties—MOR (N mm^{-2}) and MOE (N mm^{-2}; Gere and Goodno 2009). The test was carried out with a universal testing machine (SUST CMT5105, Zhuhai SUST Electrical Equipment Co., Ltd, Zhuhai, China) in which we placed a branch in the load frame, with the cross head set to move at a speed of 25 mm min^{-1}. Maximum load F_{max} (N) was determined at the point where the applied force was highest before the branch started to weaken and irreversible damage occurred. The size-independent mechanical property MOR (N mm^{-2}) was obtained with:

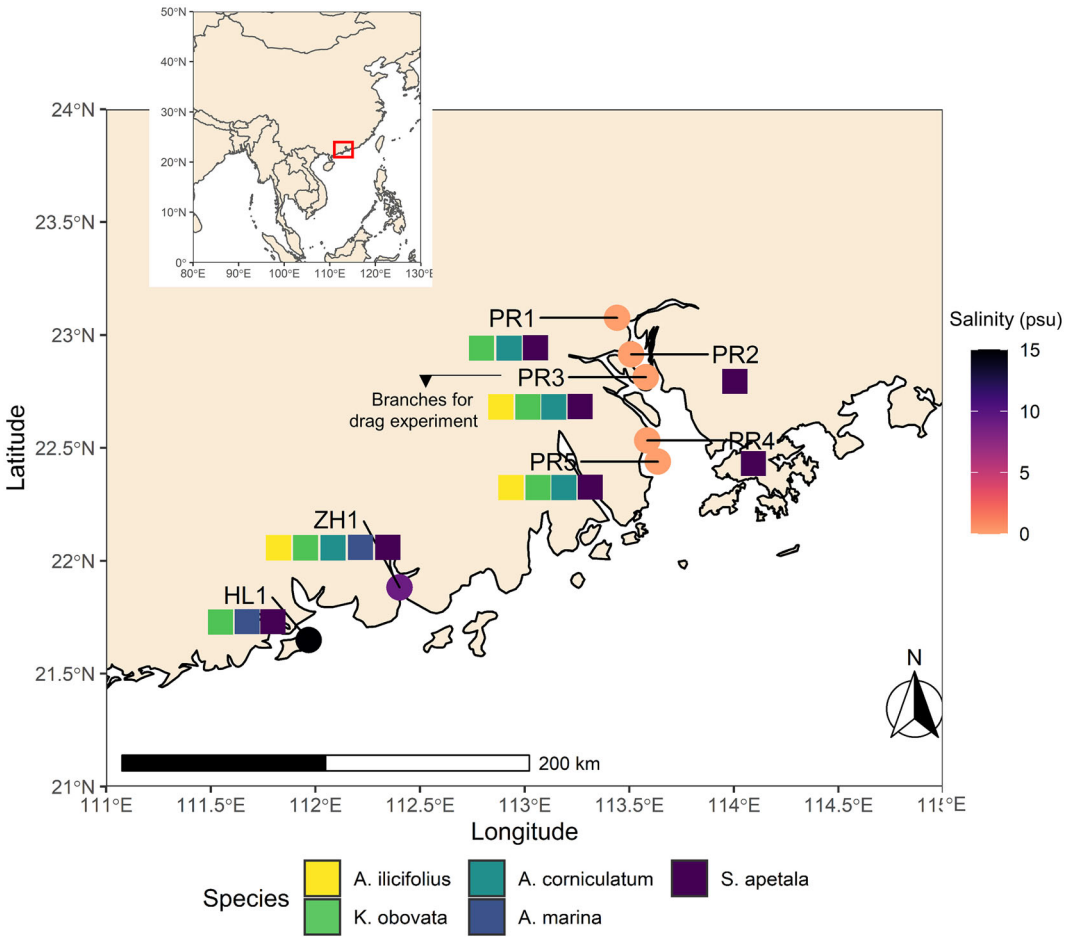

Fig 1. Site locations shown with salinity and species sampled. For details on salinity estimation, *see* Supporting Information, Appendix S1.

$$\mathrm{MOR} = \frac{F_{\max} L}{\pi R^3} \quad (1)$$

(m) undergoing loading F (N). Radius R was measured in the middle of each branch (note that branches tend to tapes), where the cross head met the branch (Fig. S4). Branches were cut so that they fit an arm of $L = \emptyset \times 20 + 2$ (to fit inside the universal testing machine and following Onoda et al. 2010 who used lengths >20 times longer than the diameter in comparable measurements), but no larger than the load frame maximum width of 38 cm. This means that branches thicker than 1.9 cm were tested with a relatively shorter arm L (68 in total). As such, we excluded these data from absolute force measurements ($F_{\max}$) as they could not be compared to other branches and only included them in relative, size-independent mechanical property measurements (MOR, MOE).

The force to bend F/x ($\mathrm{N\,mm^{-1}}$) was determined during the initial bending process where the cross head pushes down the branch before breaking. We used the initial slope of the stress–strain curve to obtain this measure (*see* Fig. S4 for an example). To obtain the size-independent mechanical property MOE ($\mathrm{N\,mm^{-2}}$), we used:

$$\mathrm{MOE} = \frac{F}{x} \times \frac{L^3}{12\pi R^4}. \quad (2)$$

Mechanical properties of mangrove leaves

Leaf mechanical properties were measured in the field during the January 2019 field campaign using a static pulling approach. For each tree of which a branch was sampled, at least five healthy, intact leaves were selected semi-randomly (i.e., with a bias for accessible leaf heights). We developed a method where we closed a thin steel wire loop around the petiole or base of the leaf (in case of a very short petiole). The other end of the wire was attached to a dynamometer with a minimum load of 0.2 kg, readability at 0.02 kg intervals, and an accuracy of ±0.08 kg (PCE-HS 50N, PCE Brookhuis, Enschede, the Netherlands). The dynamometer was then pulled at a constant speed until the leaf broke off and the peak load F_{pull} was noted. Pulled leaves were stored in plastic bags

in a cool box with ice and transferred to a fridge upon arrival at the lab, and photos and size measurements (petiole diameter, leaf width, height, and surface area) were taken within 48 h. The leaf surface area A_{leaf} (cm^2) was analyzed with photo analysis software ImageJ (Schindelin et al. 2012). Leaves were oven-dried at 60°C for 24 h. Dry weight M_{leaf} (g) of pulled leaves, averaged per tree, was used to calculate the LMA—considered a measure of investment of biomass per cm^2 leaf (Onoda et al. 2011)—as the leaf dry mass M_{leaf} per unit leaf area A_{leaf} ($LMA = M_{leaf}/A_{leaf}$, $g\,cm^{-2}$).

A measure of relative leaf attachment strength was obtained by standardizing the attachment strength against the leaf surface area A_{leaf}, where A_{leaf} can be considered a proxy for the drag forces a leaf may be experiencing (i.e., a larger leaf will experience higher drag forces; Albayrak et al. 2014):

$$MOL_A = \frac{F_{pull}}{A_{leaf}}. \quad (3)$$

A second measure of relative leaf attachment strength was obtained by standardizing the attachment strength against the LMA, to observe if leaves that require a higher investment of biomass per cm^2 (LMA) have more strongly attached leaves (higher F_{pull}):

$$MOL_M = \frac{F_{pull}}{LMA}. \quad (4)$$

Using relative measures of leaf attachment strength gives insight in whether a species invests more in leaf attachment strength F_{pull} if they have larger leaves A_{leaf}, that will inherently experience more drag, or if they have more expensive leaves, as reflected by a higher LMA. Petiole diameter was not used for calculating a relative attachment measure, as many leaves broke elsewhere; in a number of pulling attempts the whole twig with multiple leaves broke off (13% of pulling attempts for *A. marina*, 1% *K. obovata* and *S. apetala*), and in successful pulling attempts on average 72% of leaves broke off at the leaf base, such that the petiole remained attached to the tree (98% in *A. ilicifolius*, 84% in *A. corniculatum*, 81% in *A. marina*, 53% in *K. obovata*, and 42% in *S. apetala*). This might be an artifact of the pulling method, where force is concentrated in the point where the steel wire meets the leaf—under real wave loading, the interaction will be quite different, though detaching will likely require forces of a similar magnitude.

Drag force on mangrove branches

We obtained absolute (peak drag force F_D, N) and relative (drag coefficient C_D) measurements of the forces experienced by mangrove branches, the latter of which can be used to make comparisons across species. Branches of each mangrove species were sampled at the PR3 field site and tested in June 2019. For each branch, with and without leaves, we cut the branch to fit inside the flume (40 cm high × 60 cm wide). Branches were cut such that the basis of the branch matched the desired diameter; anything sticking out from the 40 × 60 cm frame was cut off. We then took a photo to measure the projected frontal surface area A_{proj} (m^2) with ImageJ (Schindelin et al. 2012). Maximum drag force F_D on branches, with and without leaves, was measured by placing the branch in a flume (located at the School of Marine Sciences, Sun Yat-Sen University, Zhuhai campus) and attaching the base of the branch to a force transducer (Load cell M140, UTILCELL, s.r.o., Ostrovačice, Czech Republic). Drag force F_D was measured for three scenarios: (1) waves without a current, (2) a current of $15\,cm\,s^{-1}$ without waves, and (3) waves and a $15\,cm\,s^{-1}$ current, with water height of 33 cm, wave height of 11 cm and a wave period of 1.5 s (achieving the highest possible conditions in this flume, resulting in around max. Orbital velocities of $0.25\,m\,s^{-1}$ for waves and currents combined with Reynolds number of about 2500). We measured current velocity at half of the water depth, which approximates the depth-averaged velocity (Hu et al. 2014; Chen et al. 2018). Following basic fluid dynamics (Morison et al. 1950), a wave-averaged drag coefficient C_D was derived from the peak drag measurements for each scenario:

$$C_D = \frac{2F_D}{\rho u^2 A_{proj}} \quad (5)$$

with u = current velocity ($m\,s^{-1}$) measured with acoustic doppler velocimeters, ρ = fluid density of freshwater ($1000\,kg\,m^{-3}$), and A_{proj} = projected frontal surface area of vegetation (m^2). We used peak drag force instead of average drag force to derive the drag coefficient, as it is the maximum force that a branch experiences that may cause breakage.

Results

Generic patterns in mangrove mechanical properties

Branch mechanical properties followed generic patterns across species, where thicker branches can withstand larger forces before breaking (F_{max}, Fig. 2a, adj. $R^2 = 0.78$, $p < 0.05$), as the volume to be broken increases cubically with branch diameter. Thicker branches also tended to be more rigid (F/x, Fig. 2b, adj. $R^2 = 0.56$, $p < 0.05$). Leaf mechanical properties also followed a generic pattern across species where leaves with a larger surface area A_{proj} or thicker petiole could withstand larger pulling forces (F_{pull}, Fig. 3c, adj. $R^2 = 0.50$; Fig. 3d, adj. $R^2 = 0.31$, $p < 0.05$). Contrarily, we did not find a generic pattern between cost of leaf production (i.e., estimated as LMA) and required pulling force to detach the leaf F_{pull} (Fig. 3g).

Variability in mechanical properties across species

We identified a trend where species that occur more seawards had significantly stronger branches but more weakly attached leaves. Firstly, this was observed for branch strength.

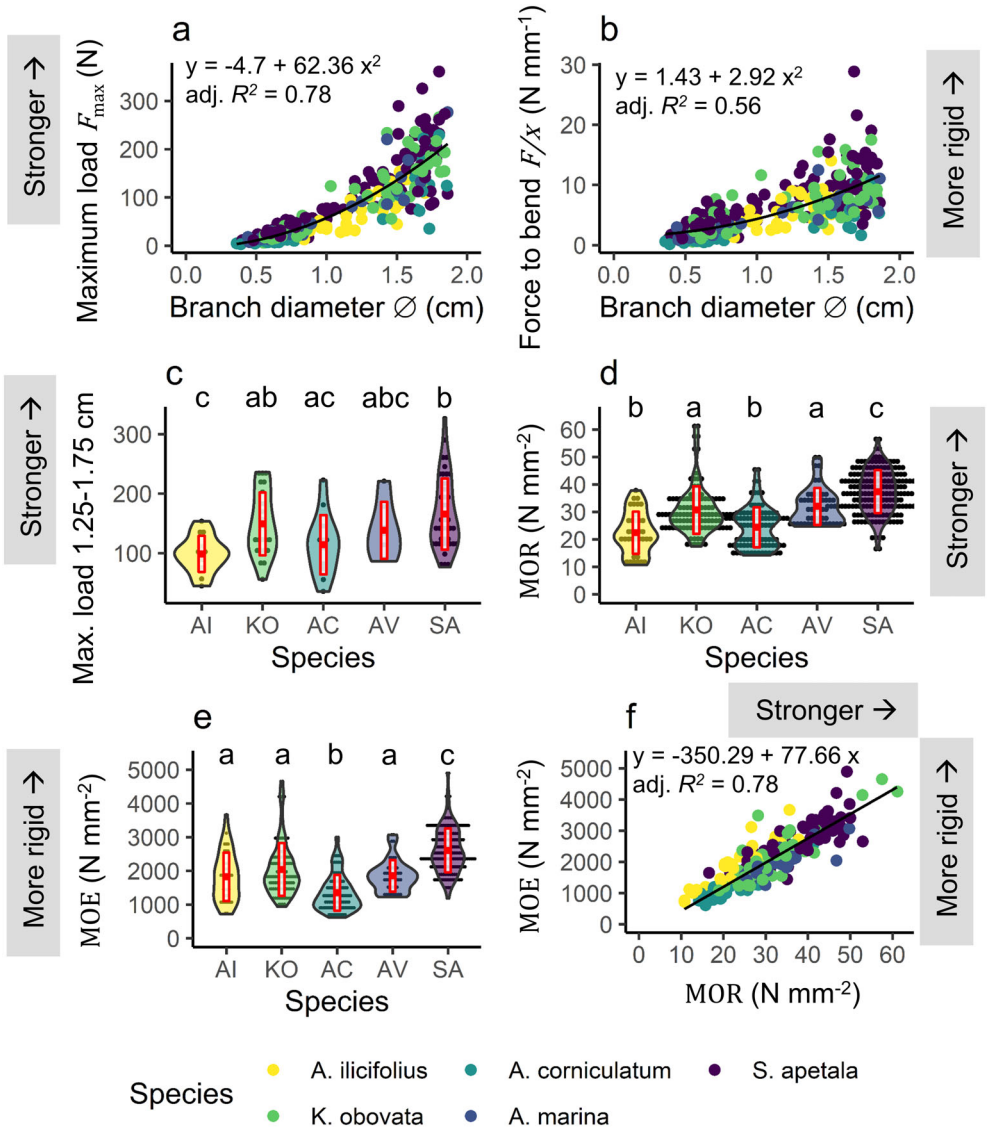

Fig 2. Branch mechanical properties of five mangrove species with (**a**) maximum load before breaking (F_{max}; N) per diameter ∅ (cm), (**b**) force needed to bend the branch (F/x; N mm^{-1}) per diameter ∅ (cm), (**c**) the maximum load F_{max} (N) for branches ranging from 1.25 to 1.75 cm, (**d**) average MOR (N mm^{-2}), (**e**) average MOE (N mm^{-2}), and (**f**) MOE vs. MOR. Red crossbars indicate mean and standard deviation. Letters indicate significance following Dunn's test with $\alpha = 0.05$.

The maximum load F_{max} that branches of 1.25–1.75 cm diameter can withstand was significantly higher for the most seaward species *S. apetala* (166.0 ± 59.9 N) compared to the most landward species *A. ilicifolius* (98.7 ± 30.4 N; Fig. 2c). The other three species fell somewhere in the middle (149.0 ± 52.9 N for *K. obovata*, 114.0 ± 50.0 N for *A. corniculatum* and 138.0 ± 47.8 N for *A. marina* branches with diameters of 1.25–1.75 cm). This pattern was also observed to some extent for the relative strength of branches, MOR, across species (Fig. 2d). Secondly, we observed significantly lower values of leaf size A_{leaf} and pulling force F_{pull} for species that generally occur more seaward (A_{leaf} 12.0 ± 2.93 cm^2 for *A. marina*, 13.7 ± 3.11 cm^2 for *S. apetala*; F_{pull} 8.73 ± 1.91 N for *A. marina*, 5.04 ± 1.67 N for *S. apetala*) vs. more landward species (A_{leaf} 33.5 ± 11.4 cm^2 and F_{pull} 15.9 ± 3.31 N for *A. ilicifolius*; Fig. 3a,b). Thirdly, we observed a significantly higher mass-based Modulus of Leaf Loss MOL_M for the landward species *A. ilicifolius* (1341 ± 505 N g^{-1} cm^2) compared to the four other species (478 ± 146 N g^{-1} cm^2 for *K. obovata*, 609 ± 159 N g^{-1} cm^2 for *A. corniculatum*, 555 ± 103 N g^{-1} cm^2 for *A. marina*, 453 ± 758 N g^{-1} cm^2 for *S. apetala*), so that *A. ilicifolius* required relatively much higher forces to detach given the investment made to produce the leaf; Fig. 3h). Finally, the trend where species that occur more seawards had significantly stronger branches but more weakly attached leaves can be observed in Fig. 4.

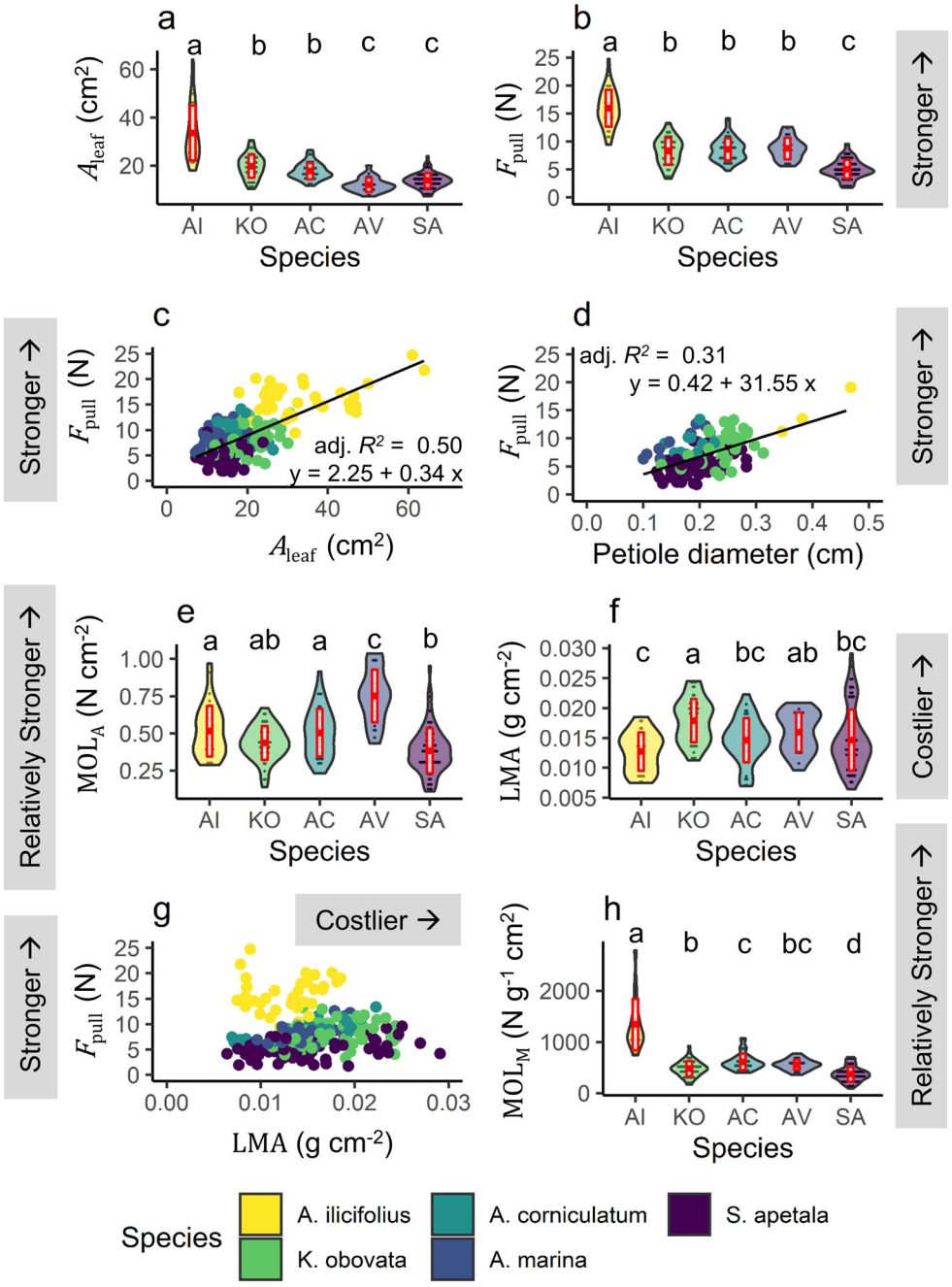

Fig 3. Leaf properties of five mangrove species with (**a**) surface area of the leaf A_{leaf} (m^2), (**b**) force needed to detach a leaf F_{pull} (N), (**c**) pulling force F_{pull} (N) vs. leaf surface area A_{leaf} (m^2), (**d**) pulling force F_{pull} (N) per petiole diameter (cm; note that *A. ilicifolius* leaves have very short petioles that broke off in 98% of pulling tests), (**e**) area-based modulus of leaf loss MOL_A as F_{pull}/A_{leaf} ($N\,cm^{-2}$), (**f**) LMA ($g\,cm^{-2}$), (**g**) LMA (i.e., considered a measure of investment of biomass per cm^2 leaf) vs puling force F_{pull} (N), and (**h**) modulus of leaf loss MOL_M as F_{pull}/LMA ($N\,g^{-1}\,cm^2$). Red crossbars indicate mean and standard deviation. Letters indicate significance following Dunn's test with $\alpha = 0.05$.

The relative flexibility, MOE, followed a less distinct pattern of increase as with distance from the coast (Fig. 2e), as *A. corniculatum* had slightly lower MOE ($1350 \pm 534\ N\ mm^{-2}$), as can also be observed in Fig. 2f. Furthermore, the relative leaf attachment strength MOL_A did not follow the seaward to landward species pattern observed above. Rather, when comparing leaf size A_{leaf} to pulling force F_{pull} (Fig. 3e), we can see that *A. marina* leaves required relatively higher force ($0.75 \pm 0.18\ N\,cm^{-2}$) to be detached given their size and may thus withstand higher drag forces than other species ($0.51 \pm 0.17\ N\,cm^{-2}$ for *A. ilicifolius*, $0.44 \pm 0.11\ N\,cm^{-2}$ for *K. obovata*, $0.50 \pm 0.16\ N\,cm^{-2}$ or *A. corniculatum*,

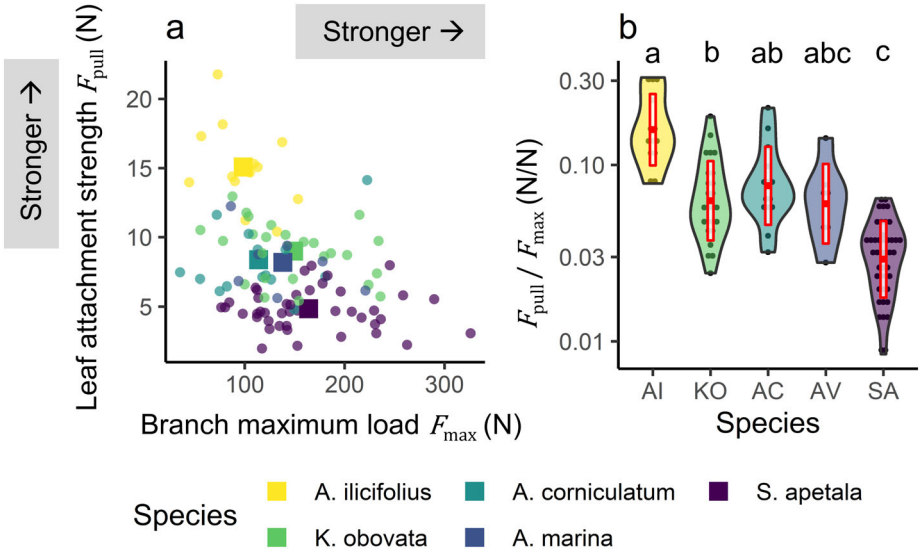

Fig 4. Relationship between absolute branch breaking strength F_{max} (N) and absolute leaf detachment strength F_{pull} (N), and the ratio between F_{pull}/F_{max} (N/N) sorted per species. Large squares represent mean values, red boxplots indicate mean and standard deviation, letters indicate significance following Dunn's test with $\alpha = 0.05$.

$0.38 \pm 0.15\,\mathrm{N\,cm^{-2}}$ for *S. apetala*). LMA did not follow a distinct pattern across species either (Fig. 3f).

Variability in mechanical properties across salinity

We identified some significant differences of mechanical properties of branches MOR and leaves F_{pull} between sites for *K. obovata*, *A. corniculatum*, and *S. apetala* and for leaves of *K. obovata*, *A. corniculatum*, and *A. marina* (Fig. 5), but found no clear correlation between salinity and mechanical properties (MOR, F_{pull}) for any species (Table S2). The observed differences between the sites were in general smaller compared to species differences (*see* Supporting Information, Appendix S1 for detailed results).

Drag force on mangrove branches

The absolute drag forces as measured on mangrove branches followed generic patterns, where branches with a larger projected surface area (A_{proj}) experienced larger drag forces F_D than smaller ones (Fig. 6), as was expected following the general drag force equation (Eq. 5). Absence of leaves drastically reduced a branch's projected surface area A_{proj} (Fig. 6), resulting in much lower drag forces F_D (Fig. 6a). Our data show a significantly higher drag coefficient C_D for *A. marina* branches (averaged across tests: 16 ± 5.99 with leaves, 5.37 ± 2.3 without leaves; Fig. 6b; Table S4), that also required relatively strong forces MOL_A to detach a leaf (Fig. 3e).

Discussion

By systematically assessing mangrove mechanical properties, we aim to contribute to the safe integration of mangrove forests in coastal flood protection structures. We measured how much force mangrove branches can experience and withstand and how this differs between mangrove species and across environments with different salinities. We observed a generic pattern across species, where thicker branches are less flexible and can withstand larger forces. We also found that larger leaves withstand larger forces before detaching from the tree. We identified a trend where species that occur more seawards have significantly stronger branches but weaker leaf attachment compared to more landward species. Across sites, we found no clear correlation between salinity and mechanical properties. Finally, drag force experienced by mangrove branches followed a generic pattern, where branches with a larger projected surface area experienced larger drag forces than smaller ones. Leaf removal drastically reduced drag force and might protect branches from breakage during a storm, making easy leaf detachment a good adaptation for pioneer species living near the forest edge.

Mechanical strategies in successional mangrove species

Coastal mangrove forests are disturbance-driven, but not all trees are damaged equally when a storm hits (Krauss and Osland 2020). Trees that grow at the seaward edge of the forest will likely be hit much harder, as the wave is still in full height. Present results suggest that the seaward dwelling pioneer species are adjusted to these harsh conditions. That is, we identified a pattern where species that generally occur more on the seaward forest edge (*S. apetala*, *A. marina*) have stronger branches yet smaller and more weakly attached leaves than landward species (*A. ilicifolius*, with *A. corniculatum* and *K. obovata* residing in between; Fig. 4). Such strong wood can resist larger forces, reducing the chance of breakage, while the weaker leaves detach more readily and thus reducing the surface area and drag force on the tree. This pattern is similar to

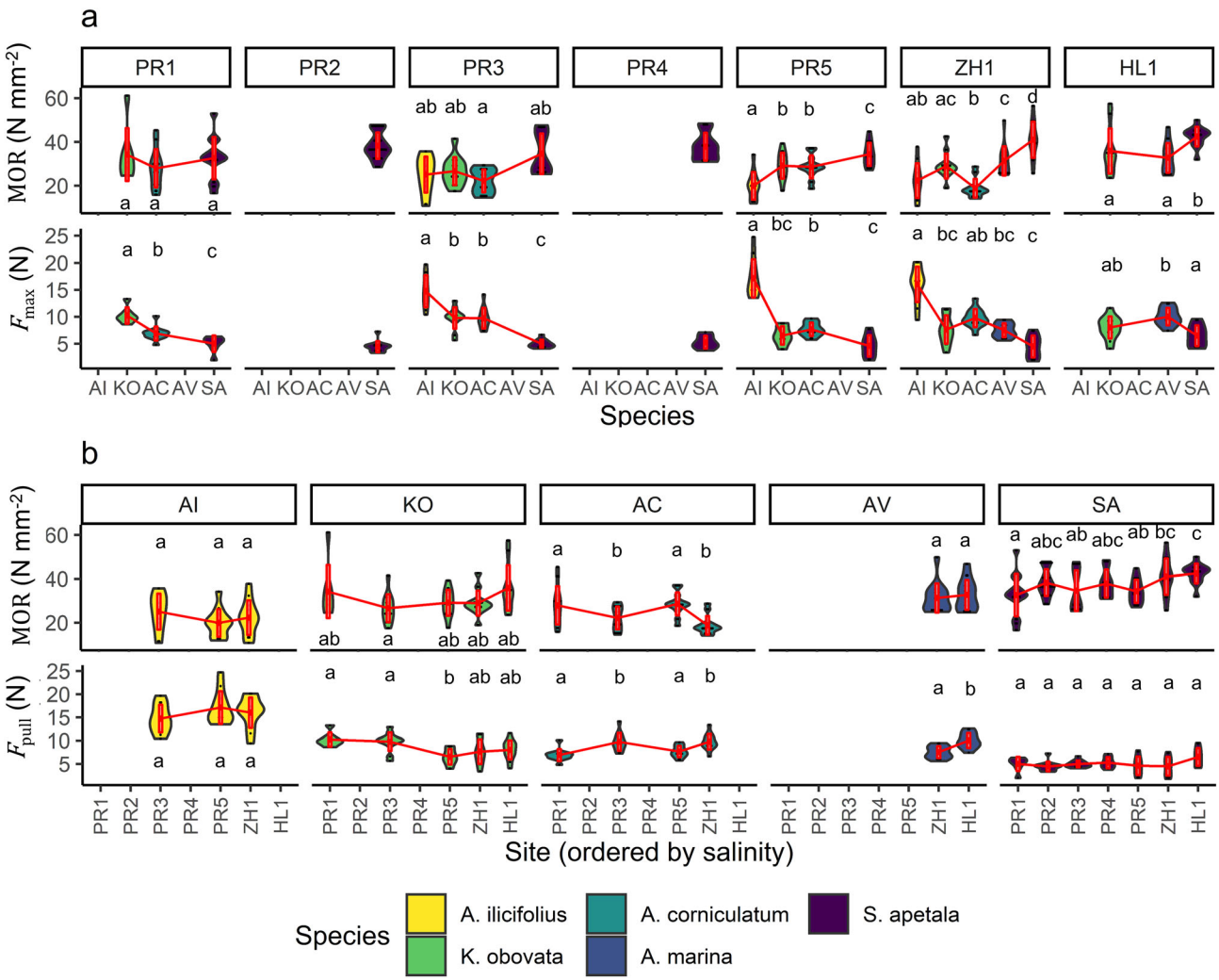

Fig 5. MOR (N mm^{-2}) and leaf strength F_{pull} (N) across (**a**) species per site and (**b**) sites per species, with sites ordered toward increasing salinity (salinity based on Fig. 1). Letters indicate significance following Dunn's test with $\alpha = 0.05$ (for *A. marina* a *t*-test was used), letters should be read per individual plot only (considering 24 plots in total).

that of intertidal marsh vegetation in temperate zones, where pioneer species also exhibit clear wave-resistance or wave-avoidance strategies (Bouma et al. 2005). We propose two possible explanations for this pattern. The first is that various species have evolved strategies to avoid damage, either through resistance or reduction of drag forces. This was studied and confirmed for 28 freshwater species, with the actual strategy (avoidance vs. tolerance) depending on the type of plant (Puijalon et al. 2011). A second explanation for the seaward vs. landward differences could be thigmomorphogenesis. Thigmomorphogenesis is the process where a plant grows smaller and more compact in response to mechanical stress such as wind or water flow (Jaffe 1973; Schoelynck et al. 2015; Gardiner et al. 2016). It is likely that plants growing at the exposed seaward edge of a mangrove forest might grow phenotypes to resist or avoid mechanical stresses. Observations on salt marsh vegetation support this hypothesis. For example, Cao et al. (2020) observed that seedlings—if they were able to survive the impact of wave exposure—developed shorter and stronger phenotypes under wave exposure. Here, we will not confirm or falsify either the evolutionary or the thigmomorphogenesis hypothesis as a driving factor behind branch and leaf strength, as (1) evolutionary studies require a different approach from our mechanistic angle (*see* Puijalon et al. 2011), and (2) the species sampling in this study was restricted by accessibility and availability within and across sites (e.g., *A. ilicifolius* was never found at exposed seaward locations). Given the findings of others described here we suspect a combination of the two will be at play.

Salinity impact on mechanical properties

Although salinity can impact wood properties (Table S1), we found no clear effect of salinity as an environmental driver of mechanical properties in mangroves across the seven sites

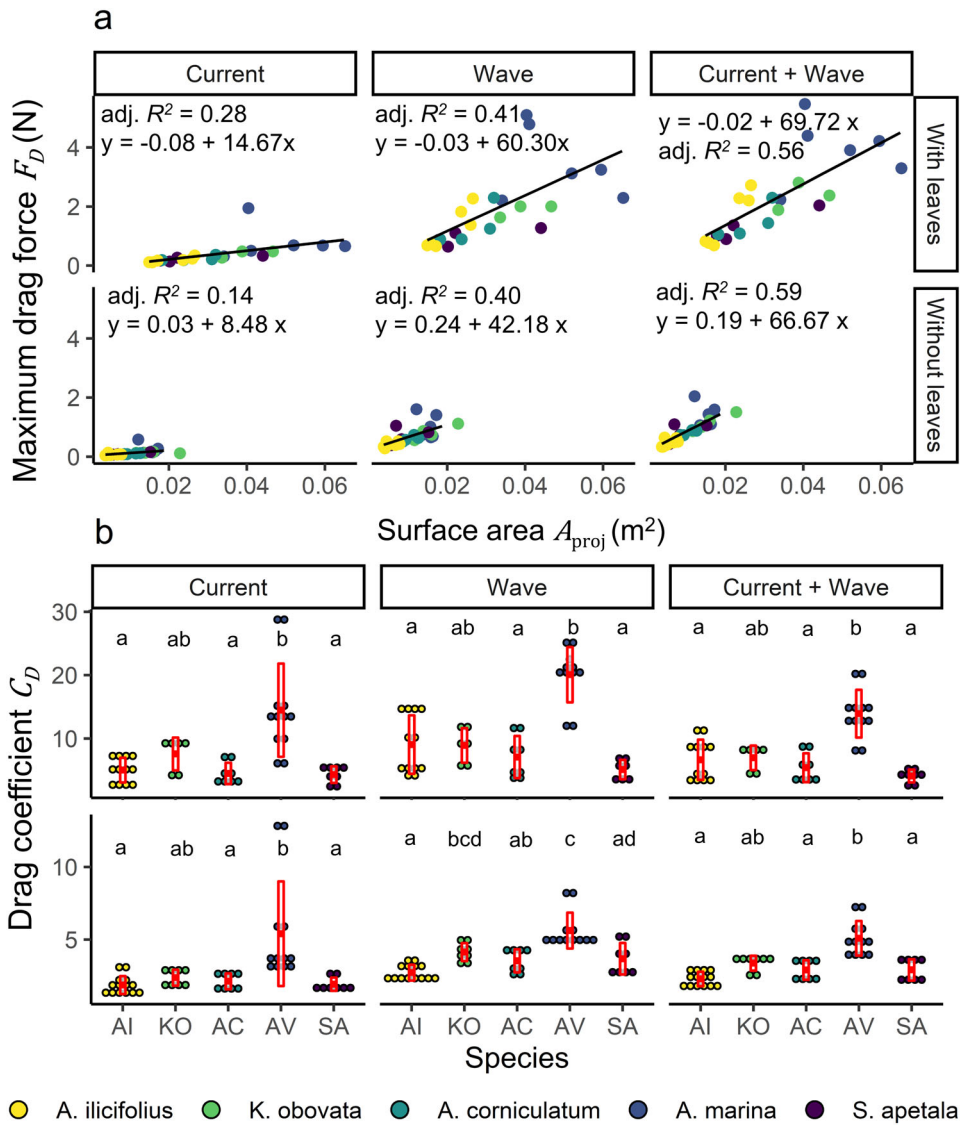

Fig 6. Drag forces and coefficients per species, with (**a**) drag force F_D (N) experienced with and without leaves per projected surface areas, and (**b**) drag coefficient C_D with and without leaves. Scenarios tested are: current only, wave only, and current with waves. Letters indicate significance following Dunn's test with $\alpha = 0.05$.

we studied. Perhaps the range of salinity across the sites we selected (estimated at 0–15 psu, *see* Supporting Information, Appendix S1) was too small to find an impact on the five species studied that had various salt tolerances (*A. ilicifolius*: low, *K. obovata*: mid, *A. corniculatum*: mid, *A. marina*: high and *S. apetala*: low; Ye et al. 2005; Reef and Lovelock 2015). Possibly, seasonal variation in salinity may have disturbed clear spatial patterns. Alternatively, there might be overruling environmental drivers at play that we were not able to identify. For example, mangroves are generally considered oligotrophic ecosystems, and the continuous terrigenous input of nutrients in the Pearl River Delta area may alter wood density (McKee 1995; Boland and Woodward 2019). Regardless, this lack of a strong salinity response simplifies modeling storm damage to mangrove forests for the studied region, as the overall patterns across the studied species are dominant.

Drag properties of mangrove branches

Larger branches are stronger, but also bigger and less flexible and experience more drag force. Furthermore, branches with a higher drag coefficient can experience larger drag forces. *A. marina* branches experienced largest drag forces and had largest drag coefficients. Note that the drag coefficients were obtained at relatively low flow velocities (around 0.25 m s^{-1} for waves and currents combined), typical to that of mangroves under normal conditions; typical flow velocities in mangrove reach 0.15–0.35 m s^{-1} during a flood tide (Mullarney et al. 2017), whereas (modeled) storm surge

conditions can produce velocities around 0.5–0.7 m s^{-1} (Fig. 7; Roeber and Bricker 2015; Dasgupta et al. 2019). Despite the low flow conditions, the tests are still informative about the drag coefficient, which is known to be reasonably constant when the Reynolds number is above 1000 (2500 in our test; Hu et al. 2014; Chen et al. 2018). However, higher flow conditions would likely result in strong branch realignment, reducing the frontal surface area and thus drag force on the branch (Vollsinger et al. 2005). Thus, the derived drag coefficients can be used as a most conservative estimate for single branches. Furthermore, we looked at drag on single branches, while surrounding vegetation causes turbulence and can increase drag forces more than twofold (Paul et al. 2016; Norris et al. 2017). Ideally, a much larger flume that can encapsulate entire tree canopies would be used to generate realistic currents and waves under variable storm surge heights or up to the point of branch or tree breakage. However, such flumes are expensive to run (Möller et al. 2014; van Wesenbeeck et al. 2021). Regardless of these limitations, *A. marina*'s larger drag coefficients are in line with their branch architecture, that is rather irregular with leaves directly attached to sturdy, inflexible branches (Fig. S6). Contrarily, *S. apetala* branches experienced much lower drag forces and have more flexible terminal branches that allow for realignment in the water stream. Aside from flexibility of branches, leaf removal also resulted in lower drag forces and drag coefficients for all species. Possibly, leaf loss can mitigate the effects of storm wind and waves, but it is not certain when this occurs. Our static measurements are useful for species comparisons but may be improved upon—to estimate leaf loss, it is necessary to know what drag forces individual leaves experience and how much they are impacted by dynamic loading from turbulent flow, which may be different from static pulling concentrated in a small point (Vogel 2009).

Mechanical tree damage during storm surges

Following methods used in mechanical storm wind damage models (Gardiner et al. 2008), our measurements of mechanical and drag properties can be used to estimate storm surge damage on idealized branches. Here, we can compare the drag force generated under different wave orbital velocities to the maximum force a branch can withstand. A branch will break if the drag force (F_D) it experiences becomes larger than the maximum force ($F_{\max}$) it can withstand. This maximum strength will depend on the relative strength of the wood (MOR) and the branch arm the drag force is acting on (L) (Eq. S1, Appendix S1). The drag force the branch experiences will depend on the projected frontal surface area of the branch (A_{proj}), the drag coefficient (C_D), and the flow velocity (u) (Eq. S2, Appendix S1). We show an example of such an estimation for idealized branches that are rigid and completely submerged in Fig. 7 (*see* Supporting Information, Appendix S1 for the full calculation). When scaling up to full trees, a similar approach may be used where the diameter of the idealized branch becomes the diameter of the idealized trunk. There are a number of steps that can be taken to refine this simple model. First, one can validate that the MOR for branches (0.5–1.75 cm diameter) remains the same for tree trunks (Fig. S1) by measuring the MOR of tree trunks directly—but carefully, so that no vulnerable mangrove forests are harmed. Second, one can link drag coefficients more closely to natural conditions by including surrounding vegetation in drag measurements,

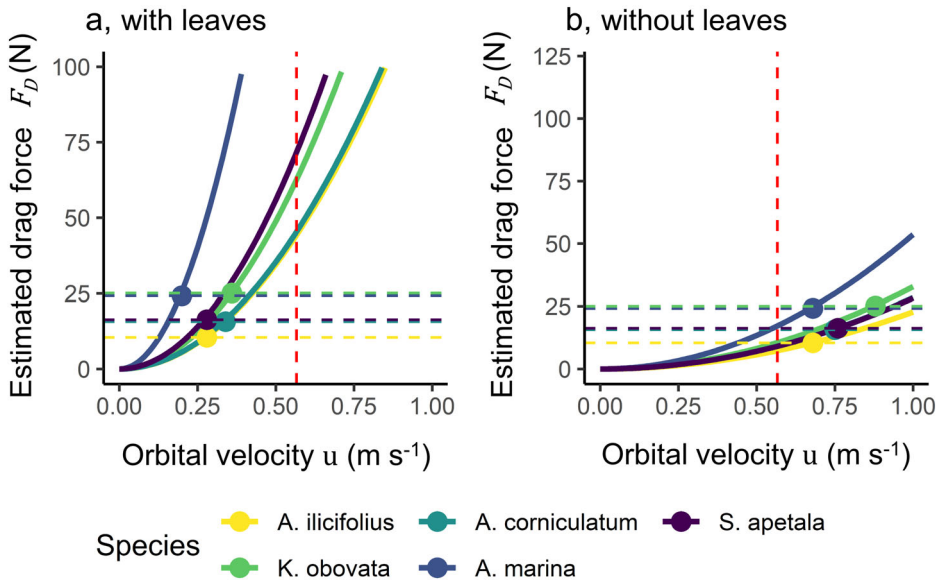

Fig 7. Conceptual model with estimations of drag force F_D experienced for idealized branches of 1 cm in diameter ∅, (**a**) with and (**b**) without leaves. Dashed lines indicated maximum force $F_{\max}$ a branch can withstand. Red dotted lines indicate estimated peak orbital velocity during a typhoon (based on Hato, August 2017). *See* Supporting information, Appendix S1 for calculation.

as discussed in the previous Section, or by measuring drag in the field. Third, one can include how the realignment of branches and leaves impacts the frontal surface area A_{proj} or arm L. In three North American hardwood species placed in a wind tunnel under wind velocities of $20\,m\,s^{-1}$, branch realignment resulted in a 50% reduction in projected frontal surface area (Vollsinger et al. 2005). Fourth, one may consider the tree location and average height distribution of branches and leaves per species relative to (variable) storm surge heights. For example, late-successional species are generally located higher in the intertidal zone, where they may be less submerged by a storm surge, and more sheltered from storm waves. However, in the Pearl River Delta, the average height of native trees is comparable to that of the seawalls behind them, and can thus experience waves over the full height of the tree during storms. Depending on whether it is wind or waves that will reach branches during a storm, drag properties in wind will also need to be included in the model. Fifth, trees can experience much larger loads from dynamic loading than static loading (James et al. 2013). Measuring dynamic loads is currently not possible, given the lack of knowledge on motion. Thus, measuring the difference between static vs. dynamic loading on mangrove trees and branches should be addressed in future research. Furthermore, aside from breaking mechanisms, uprooting mechanisms should also be included, particularly if storms are accompanied by large erosion events that can result in the loss of a tree's mechanical stability (Gardiner et al. 2016). Last, measuring what drag forces leaves experience under real wind and wave loads and when leaf loss occurs will help us understand if trees will experience complete defoliation, which can be lethal, particularly in species that cannot resprout epicormically (e.g., Rhizophoraceae, Gill and Tomlinson 1969; Saenger 2002).

Toward long-term coastal flood safety with mangrove forests

This research provides a basis for understanding the mechanistic processes that take place in mangrove forests during major storms. It provides a comprehensive dataset of mechanical and drag properties of mangrove species in one of the most highly urbanized, at-risk urban deltas in the world. This is a key input to model assessment and an important step in the direction of analytical storm damage modeling in mangroves. This research also produces new insights in damage-resistance strategies across mangrove species. These results may provide guidance on mangrove afforestation efforts for flood protection, suggesting that pioneer species are more suitable to resist the influence of the exposed seaward environment. This amplifies knowledge that pioneer species are generally more suitable to grow in the lower intertidal zone (Lewis 2005; Primavera et al. 2016). In the case of the Pearl River Delta, we emphasize that *S. apetala* is an introduced and potentially invasive species and its long-term impact on natural ecosystem functioning is not fully understood (Ren et al. 2009). Thus, care should be taken in species selection when afforesting for long-term flood defense.

Ultimately, long-term flood protection will require scaling up individual tree damage to whole-ecosystem damage and taking into account the indirect impacts of storms such as prolonged flooding and sedimentation (Krauss and Osland 2020). It should also consider other drivers of variability across species and space, such as regeneration speeds between species (Gill and Tomlinson 1969; Saenger 2002) or changes in tidal regime or salinity, which could alter species zonation in the coastal zone and consequently change the storm resistance of the present ecosystem (Zhu et al. 2019). As more knowledge is gained about mechanical tree damage, it will become easier to predict forest structure and size over time and provide reliable long-term flood safety predictions. This will advance the incorporation of nature in flood defense schemes and enable affordable and durable coastal flood safety while preserving one of the most precious ecosystems on earth.

References

Albayrak, I., V. Nikora, O. Miler, and M. T. O'Hare. 2014. Flow–plant interactions at leaf, stem and shoot scales: Drag, turbulence, and biomechanics. Aquat. Sci. **76**: 269–294. doi:10.1007/s00027-013-0335-2

Bao, T. Q. 2011. Effect of mangrove forest structures on wave attenuation in coastal Vietnam. Oceanologia **53**: 807–818. doi:10.5697/oc.53-3.807

Boland, J. M., and D. L. Woodward. 2019. Impacts of the invasive shot hole borer (*Euwallacea kuroshio*) are linked to sewage pollution in southern California: The enriched tree hypothesis. PeerJ **2019**: 1–22. doi:10.7717/peerj.6812

Borsje, B. W., B. K. van Wesenbeeck, F. Dekker, P. Paalvast, T. J. Bouma, M. M. van Katwijk, and M. B. de Vries. 2011. How ecological engineering can serve in coastal protection. Ecol. Eng. **37**: 113–122. doi:10.1016/j.ecoleng.2010.11.027

Bouma, T. J., and others. 2014. Identifying knowledge gaps hampering application of intertidal habitats in coastal protection: Opportunities & steps to take. Coast. Eng. **87**: 147–157. doi:10.1016/j.coastaleng.2013.11.014

Bouma, T. J., M. B. De Vries, E. Low, G. Peralta, I. C. Tánczos, J. Van De Koppel, and P. M. J. Herman. 2005. Trade-offs related to ecosystem engineering: A case study on stiffness of emerging macrophytes. Ecology **86**: 2187–2199. doi:10.1890/04-1588

Butler, D. W., S. M. Gleason, I. Davidson, Y. Onoda, and M. Westoby. 2012. Safety and streamlining of woody shoots in wind: An empirical study across 39 species in tropical Australia. New Phytol. **193**: 137–149. doi:10.1111/j.1469-8137.2011.03887.x

Cao, H., Z. Zhu, R. James, P. M. J. Herman, L. Zhang, L. Yuan, and T. J. Bouma. 2020. Wave effects on seedling establishment of three pioneer marsh species: Survival, morphology

and biomechanics. Ann. Bot. **125**: 345–352. doi:10.1093/aob/mcz136

Chave, J., D. Coomes, S. Jansen, S. L. Lewis, N. G. Swenson, and A. E. Zanne. 2009. Towards a worldwide wood economics spectrum. Ecol. Lett. **12**: 351–366. doi:10.1111/j.1461-0248.2009.01285.x

Chen, Q., J. Li, L. Zhang, H. Lu, H. Ren, and S. Jian. 2015. Changes in the macrobenthic faunal community during succession of a mangrove forest at Zhanjiang, South China. J. Coast. Res. **300**: 315–325. doi:10.2112/jcoastres-d-13-00019.1

Chen, H., and others. 2018. Deriving vegetation drag coefficients in combined wave-current flows by calibration and direct measurement methods. Adv. Water Resour. **122**: 217–227. doi:10.1016/j.advwatres.2018.10.008

CIRIA, Ministere de l'Ecologie, du Developpement durable et de l'Energie, and US Army Corps of Engineers. 2013. The international levee handbook. CIRIA.

Dasgupta, S., M. S. Islam, M. Huq, Z. H. Khan, and M. R. Hasib. 2019. Quantifying the protective capacity of mangroves from storm surges in coastal Bangladesh I.A. Kimirei [ed.]. PLoS ONE **14**: e0214079. doi:10.1371/journal.pone.0214079

Denny, M., and B. Gaylord. 2002. Review the mechanics of wave-swept algae. J. Exp. Biol. **205**: 1355–1362.

De Dominicis, M., J. Wolf, S. Jevrejeva, P. Zheng, and Z. Hu. 2020. Future interactions between sea level rise, tides, and storm surges in the world's largest urban area. Geophys. Res. Lett. **47**: 1–11. doi:10.1029/2020GL087002

Gardiner, B., P. Berry, and B. Moulia. 2016. Review: Wind impacts on plant growth, mechanics and damage. Plant Sci. **245**: 94–118. doi:10.1016/j.plantsci.2016.01.006

Gardiner, B., K. Byrne, S. Hale, K. Kamimura, S. J. Mitchell, H. Peltola, and J. C. Ruel. 2008. A review of mechanistic modelling of wind damage risk to forests. Forestry **81**: 447–463. doi:10.1093/forestry/cpn022

Gere, J. M., and B. J. Goodno. 2009. Mechanics of materials. Cengage Learning.

Gill, A. M., and P. B. Tomlinson. 1969. Studies on the growth of Red Mangrove (*Rhizophora mangle* L.) I. Habit and general morphology. Biotropica **1**: 1. doi:10.2307/2989744

Hoegh-Guldberg, O.D., and others. 2018. Impacts of 1.5 C global warming on natural and human systems. Global warming of 1.5 C. An IPCC special report. IPCC Secretariat.

Horstman, E. M., C. M. Dohmen-Janssen, P. M. F. Narra, N. J. F. van den Berg, M. Siemerink, and S. J. M. H. Hulscher. 2014. Wave attenuation in mangroves: A quantitative approach to field observations. Coast. Eng. **94**: 47–62. doi:10.1016/j.coastaleng.2014.08.005

Hu, Z., T. Suzuki, T. Zitman, W. Uittewaal, and M. Stive. 2014. Laboratory study on wave dissipation by vegetation in combined current-wave flow. Coast. Eng. **88**: 131–142. doi:10.1016/j.coastaleng.2014.02.009

Jaffe, M. J. 1973. Thigmomorphogenesis: The response of plant growth and development to mechanical stimulation. Planta (Berh) **114**: 143–157. doi:10.1007/BF00387472

James, K., C. Hallam, and C. Spencer. 2013. Measuring tilt of tree structural root zones under static and wind loading. Agric. For. Meteorol. **168**: 160–167. doi:10.1016/j.agrformet.2012.09.009

Jie, Y., W. Shaohong, and D. Erfu. 2012. Assessment of economic damage risks from typhoon disasters in Guangdong, China. J. Resour. Ecol. **3**: 144–150. doi:10.5814/j.issn.1674-764x.2012.02.006

Jimenez, J. A., A. E. Lugo, and G. Cintron. 1985. Tree mortality in mangrove forests. Biotropica **17**: 177. doi:10.2307/2388214

Johnstone, J. F., and others. 2016. Changing disturbance regimes, ecological memory, and forest resilience. Front. Ecol. Environ. **14**: 369–378. doi:10.1002/fee.1311

Kauffman, J. B., and T. G. Cole. 2010. Micronesian mangrove forest structure and tree responses to a severe typhoon. Wetlands **30**: 1077–1084. doi:10.1007/s13157-010-0114-y

Knutson, T., and others. 2019. Tropical cyclones and climate change assessment: Part II. Projected response to anthropogenic warming. Bull. Am. Meteorol. Soc. **101**: 1–62. doi:10.1175/bams-d-18-0194.1

Koch, E. W., and others. 2009. Non-linearity in ecosystem services: Temporal and spatial variability in coastal protection. Front. Ecol. Environ. **7**: 29–37. doi:10.1890/080126

Krauss, K. W., and M. J. Osland. 2020. Tropical cyclones and the organization of mangrove forests: A review. Ann. Bot. **125**: 213–234. doi:10.1093/aob/mcz161

Lee, S. Y., and others. 2014. Ecological role and services of tropical mangrove ecosystems: A reassessment. Glob. Ecol. Biogeogr. **23**: 726–743. doi:10.1111/geb.12155

Lewis, R. R. 2005. Ecological engineering for successful management and restoration of mangrove forests. Ecol. Eng. **24**: 403–418. doi:10.1016/j.ecoleng.2004.10.003

Mazda, Y., M. Magi, M. Kogo, and P. N. Hong. 1997. Mangroves as a coastal protection from waves in the Tong King Delta, Vietnam. Mangroves Salt Marshes **1**: 127–135. doi:10.1023/A:1009928003700

McIvor, A., T. Spencer, M. Spalding, C. Lacambra, and I. Möller. 2015. Mangroves, tropical cyclones, and coastal hazard risk reduction, p. 403–429. *In* Coastal and marine hazards, risks, and disasters. Elsevier.

McKee, K. L. 1995. Interspecific variation in growth, biomass partitioning, and defensive characteristics of neotropical mangrove seedlings: Response to light and nutrient availability. Am. J. Bot. **82**: 299–307. doi:10.2307/2445575

Menéndez, P., I. J. Losada, S. Torres-Ortega, S. Narayan, and M. W. Beck. 2020. The global flood protection benefits of mangroves. Sci. Rep. **10**: 1–11. doi:10.1038/s41598-020-61136-6

Möller, I., M and others. 2014. Wave attenuation over coastal salt marshes under storm surge conditions. Nat. Geosci. **7**: 727–731. doi:10.1038/ngeo2251

Morison, J. R., J. W. Johnson, and S. A. Schaaf. 1950. The force exerted by surface waves on piles. J. Petrol. Tech. **2**: 149–154. doi:10.2118/950149-G

Morris, R. L., E. M. A. Strain, T. M. Konlechner, B. J. Fest, D. M. Kennedy, S. K. Arndt, and S. E. Swearer. 2019. Developing a nature-based coastal defence strategy for Australia. Aust. J. Civ. Eng. **17**: 167–176. doi:10.1080/14488353.2019.1661062

Mullarney, J. C., S. M. Henderson, J. A. H. Reyns, B. K. Norris, and K. R. Bryan. 2017. Spatially varying drag within a wave-exposed mangrove forest and on the adjacent tidal flat. Cont. Shelf Res. **147**: 102–113. doi:10.1016/j.csr.2017.06.019

Nicholls, R. J., J. Hinkel, D. Lincke, and T. van der Pol. 2019. Global investment costs for coastal defense through the 21st century. The World Bank.

Norris, B. K., J. C. Mullarney, K. R. Bryan, and S. M. Henderson. 2017. The effect of pneumatophore density on turbulence: A field study in a Sonneratia-dominated mangrove forest. Vietnam. Cont. Shelf Res. **147**: 114–127. doi:10.1016/j.csr.2017.06.002

Onoda, Y., A. E. Richards, and M. Westoby. 2010. The relationship between stem biomechanics and wood density is modified by rainfall in 32 Australian woody plant species. New Phytol. **185**: 493–501. doi:10.1111/j.1469-8137.2009.03088.x

Onoda, Y. M., and others. 2011. Global patterns of leaf mechanical properties. Ecol. Lett. **14**: 301–312. doi:10.1111/j.1461-0248.2010.01582.x

Ouyang, X., F. Guo, and S. Y. Lee. 2021. The impact of super-typhoon Mangkhut on sediment nutrient density and fluxes in a mangrove forest in Hong Kong. Sci. Total Environ. **766**: 142637. doi:10.1016/j.scitotenv.2020.142637

Paul, M., and others. 2016. Plant stiffness and biomass as drivers for drag forces under extreme wave loading: A flume study on mimics. Coast. Eng. **117**: 70–78. doi:10.1016/j.coastaleng.2016.07.004

Peltola, H., S. Kellomäki, H. Väisänen, and V. P. Ikonen. 1999. A mechanistic model for assessing the risk of wind and snow damage to single trees and stands of scots pine, Norway spruce, and birch. Can. J. For. Res. **29**: 647–661. doi:10.1139/x99-029

Peng, Y., and others. 2016. Virtual increase or latent loss? A reassessment of mangrove populations and their conservation in Guangdong, southern China. Mar. Pollut. Bull. **109**: 691–699. doi:10.1016/j.marpolbul.2016.06.083

Primavera, J. H., and others. 2016. Preliminary assessment of post-Haiyan mangrove damage and short-term recovery in Eastern Samar, Central Philippines. Mar. Pollut. Bull. **109**: 744–750. doi:10.1016/j.marpolbul.2016.05.050

Puijalon, S., T. J. Bouma, C. J. Douady, J. van Groenendael, N. P. R. Anten, E. Martel, and G. Bornette. 2011. Plant resistance to mechanical stress: Evidence of an avoidance-tolerance trade-off. New Phytol. **191**: 1141–1149. doi:10.1111/j.1469-8137.2011.03763.x

Reef, R., and C. E. Lovelock. 2015. Regulation of water balance in mangroves. Ann. Bot. **115**: 385–395. doi:10.1093/aob/mcu174

Ren, H., S. Jian, H. Lu, Q. Zhang, W. Shen, W. Han, Z. Yin, and Q. Guo. 2008. Restoration of mangrove plantations and colonisation by native species in Leizhou bay, South China. Ecol. Res. **23**: 401–407. doi:10.1007/s11284-007-0393-9

Ren, H., H. Lu, W. Shen, C. Huang, Q. Guo, Z. Li, and S. Jian. 2009. *Sonneratia apetala* Buch. Ham in the mangrove ecosystems of China: An invasive species or restoration species? Ecol. Eng. **35**: 1243–1248. doi:10.1016/j.ecoleng.2009.05.008

Roeber, V., and J. D. Bricker. 2015. Destructive tsunami-like wave generated by surf beat over a coral reef during typhoon Haiyan. Nat. Commun. **6**: 7854. doi:10.1038/ncomms8854

Saenger, P. 2002. Mangrove ecology, silviculture and conservation. Springer Science & Business Media.

Santini, N. S., N. Schmitz, V. Bennion, and C. E. Lovelock. 2013. The anatomical basis of the link between density and mechanical strength in mangrove branches. Funct. Plant Biol. **40**: 400–408. doi:10.1071/FP12204

Santini, N. S., N. Schmitz, and C. E. Lovelock. 2012. Variation in wood density and anatomy in a widespread mangrove species. Trees Struct. Funct. **26**: 1555–1563. doi:10.1007/s00468-012-0729-0

Scheffer, M., S. Carpenter, J. A. Foley, C. Folke, and B. Walker. 2001. Catastrophic shifts in ecosystems. Nature **413**: 591–596. doi:10.1038/35098000

Schindelin, J., and others. 2012. Fiji: An open-source platform for biological-image analysis. Nat. Methods **9**: 676–682.

Schoelynck, J., S. Puijalon, P. Meire, and E. Struyf. 2015. Thigmomorphogenetic responses of an aquatic macrophyte to hydrodynamic stress. Front. Plant Sci. **6**: 1–7. doi:10.3389/fpls.2015.00043

Schoutens, K., M. Heuner, E. Fuchs, V. Minden, T. Schulte-Ostermann, J.-P. Belliard, T. J. Bouma, and S. Temmerman. 2020. Nature-based shoreline protection by tidal marsh plants depends on trade-offs between avoidance and attenuation of hydrodynamic forces. Estuar. Coast. Shelf Sci. **236**: 106645. doi:10.1016/j.ecss.2020.106645

Simard, M., L. Fatoyinbo, C. Smetanka, V. H. Rivera-Monroy, E. Castañeda-Moya, N. Thomas, and T. Van der Stocken. 2019. Mangrove canopy height globally related to precipitation, temperature and cyclone frequency. Nat. Geosci. **12**: 40–45. doi:10.1038/s41561-018-0279-1

Smith, T. J., M. B. Robblee, H. R. Wanless, and T. W. Doyle. 1994. Mangroves, hurricanes and lightning strikes. Bioscience **44**: 256–262. doi:10.2307/1312230

Tanaka, K. 2008. Effectiveness and limitation of the coastal vegetation for storm surge disaster mitigation. Investigation report on the storm surge disaster by Cyclone Sidr in 2007, Bangladesh. Investigation Team of Japan Society of Civil Engineering. http://www.jsce.or.jp/report/46/files/Bangladesh_Investigation.pdf.

Temmerman, S., P. Meire, T. J. Bouma, P. M. J. Herman, T. Ysebaert, and H. J. De Vriend. 2013. Ecosystem-based coastal defence in the face of global change. Nature **504**: 79–83. doi:10.1038/nature12859

Vogel, S. 2009. Leaves in the lowest and highest winds: Temperature, force and shape. New Phytol. **183**: 13–26. doi:10.1111/j.1469-8137.2009.02854.x

Vollsinger, S., S. J. Mitchell, K. E. Byrne, M. D. Novak, and M. Rudnicki. 2005. Wind tunnel measurements of crown streamlining and drag relationships for several hardwood species. Can. J. For. Res. **35**: 1238–1249. doi:10.1139/x05-051

van Wesenbeeck, B. K., and others. 2017. Implementing nature based flood protection: Principles and implementation guidance. World Bank.

van Wesenbeeck, B. K., G. Wolters, J. A. A. Antolínez, S. Kalloe, B. Hofland, W. de Boer, C. Çete, and T. J. Bouma. 2021. Woods versus waves: Wave attenuation through non-uniform forests under extreme conditions. Res. Square. doi:10.21203/rs.3.rs-321272/v1

Xin, K., Q. Zhou, S. K. Arndt, and X. Yang. 2013. Invasive capacity of the mangrove Sonneratia apetala in Hainan Island, China. J. Trop. For. Sci. **25**: 70–78.

Yin, K., S. Xu, W. Huang, and Y. Xie. 2017. Effects of sea level rise and typhoon intensity on storm surge and waves in Pearl River Estuary. Ocean Eng. **136**: 80–93. doi:10.1016/j.oceaneng.2017.03.016

Ye, Y., N. F.-Y. Tam, C.-Y. Lu, and Y.-S. Wong. 2005. Effects of salinity on germination, seedling growth and physiology of three salt-secreting mangrove species. Aquat. Bot. **83**: 193–205. doi:10.1016/j.aquabot.2005.06.006

Zhu, Z., Z. Yang, and T. J. Bouma. 2019. Biomechanical properties of marsh vegetation in space and time: Effects of salinity, inundation and seasonality. Ann. Bot.: **125**: 1–13. doi:10.1093/aob/mcz063

Acknowledgments

We would like to thank Juangling Zhou and Simei Lian with their help to execute experiments and Peng Zheng for providing us salinity and orbital velocity model outputs, the Qiao Island Mangrove Reserve and the Hailing Island Mangrove Wetland Park for allowing us to do field work, and the mechanical lab at Sun Yat-Sen University, Zhuhai campus, for letting us use their universal testing machine. The authors gratefully acknowledge financial supports of the Joint Research Project: NSFC (51761135022), NWO (ALWSD.2016.026), and EPSRC (EP/R024537/1): Sustainable Deltas, and Guangdong Provincial Department of Science and Technology (2019ZT08G090), and of the Innovation Group Project of Southern Marine Science and Engineering Guangdong Laboratory (Zhuhai) (No. 311021004), Guangdong Provincial Department of Science and Technology (2019ZT08G090) and Fundamental Research Funds for the Central Universities of China (20lgzd16). The data can be found at https://doi.org/10.25850/nioz/7b.b.jb.

Conflict of interest

None declared.

Submitted 09 November 2020
Revised 13 April 2021
Accepted 06 June 2021

Deputy editor: Julia Mullarney